The impact of igneous bedrock weathering on the Mo isotopic composition of stream waters: Natural samples and laboratory experiments

Andrea R Voegelin, Thomas Nagler, Thomas Pettke, Nadja Neubert, Marc Steinmann, Olivier Pourret, Igor M Villa

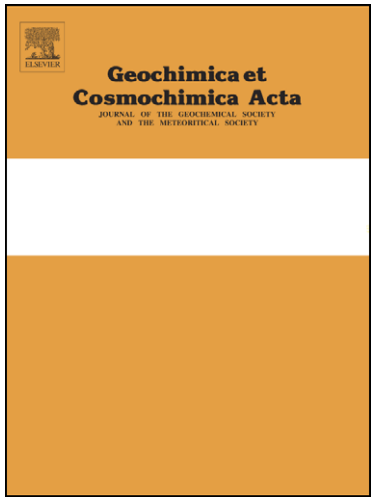

The impact of igneous bedrock weathering on the Mo isotopic composition of stream waters : Natural samples and laboratory experiments

Andrea R. Voegelin, Thomas F. Nägler, Thomas Pettke, Nadja Neubert, Marc Steinmann, Olivier Pourret, Igor M. Villa

PII: S0016-7037(12)00127-5
DOI: 10.1016/j.gca.2012.02.029
Reference: GCA 7632

To appear in: *Geochimica et Cosmochimica Acta*

Received Date: 28 July 2011
Accepted Date: 26 February 2012

Please cite this article as: Voegelin, A.R., Nägler, T.F., Pettke, T., Neubert, N., Steinmann, M., Pourret, O., Villa, I.M., The impact of igneous bedrock weathering on the Mo isotopic composition of stream waters : Natural samples and laboratory experiments, *Geochimica et Cosmochimica Acta* (2012), doi: 10.1016/j.gca.2012.02.029

The impact of igneous bedrock weathering on the Mo isotopic composition of stream waters : Natural samples and laboratory experiments

Andrea R. Voegelin[a,*], Thomas F. Nägler[a], Thomas Pettke[a], Nadja Neubert[b], Marc Steinmann[c], Olivier Pourret[d], Igor M. Villa[a,e]

[a] *Institut für Geologie, Universität Bern, Baltzerstrasse 3, CH-3012 Bern, Switzerland*
[b] *Leibniz Universität Hannover, Institut für Mineralogie, Callinstrasse 3, D-30167 Hannover, Germany*
[c] *UMR 6249 Chrono-Environnement, Université de Franche-Comté, F-25030 Besançon, France*
[d] *Institut Polytechnique LaSalle-Beauvais, Département de Géosciences, 19 rue Pierre Waguet, F-60026 Beauvais Cedex, France*
[e] *Dipartimento di Scienze Geologiche e Geotecnologie, Università di Milano Bicocca, I-20126 Milano, Italy*

Abstract

River waters have been shown to be systematically enriched in the heavy molybdenum (Mo) isotopes when compared to typical granites and basalts, which generally possess Mo isotopic compositions ($\delta^{98/95}$Mo) of around 0‰. This inconsistency has been used to argue against weathering of crustal rocks as the cause for heavy riverine $\delta^{98/95}$Mo signatures. Incongruent dissolution of primary bedrock, however, may be an important process by which the anomalous Mo signatures of the river dissolved load are produced. This study therefore investigates the effect of igneous crustal rock weathering on the aquatic $\delta^{98/95}$Mo signal by comparing stream water and bedrock Mo isotope data to results of bulk rock leach experiments. For this purpose, stream water and bedrock (orthogneiss, granite, basalt), as well as soil and vegetation samples were collected in a small catchment in the French Massif Central. In accordance with the results of earlier studies on riverine Mo, both streams are isotopically heavier ($\delta^{98/95}$Mo = 0.5 to 1.1‰) than the typical granites and basalts. The excellent agreement of these data with those of Mo released during experimental leaching

*Corresponding author Tel: +41 61 631 85 33 Fax: +41 31 631 48 43
Email address: voegelin@geo.unibe.ch (Andrea R. Voegelin)

of the basalt bedrock (0.6 to 1.0‰) identifies a predominance of basalt weathering over the stream water Mo geochemistry, while other processes (i.e. soil formation, secondary mineral precipitation and adsorption) are subordinate in this catchment. Given that the basalt bulk rock $\delta^{98/95}$Mo reflects a value typical for crustal magmatic rocks (ca. 0.1‰), Mo isotope fractionation during the incongruent dissolution of basalt can explain the observed isotopically heavy aquatic Mo signatures. Laser ablation analyses demonstrate that the volumetrically minor magmatic sulfides can be highly enriched in Mo and mass balance calculations identify the sulfide melt inclusions as the principal Mo source for the leach solutions. These data suggest that the magmatic sulfides possess a distinctly heavier $\delta^{98/95}$Mo signature than the coexisting silicate melt. In this case, Mo would behave like Fe by showing a detectable isotope fractionation at magmatic temperatures. Incongruent crustal bedrock weathering may thus cause a preferential release of heavy Mo isotopes. This effect, however, is highly dependent on the primary bedrock mineralogy. Consequently, the average continental runoff may have been significantly affected by incongruent weathering during periods when the Earth system was exceptionally far from steady state, e.g., large glaciations with enhanced physical weathering or large subaerial basalt eruptions such as the Deccan and the Siberian plateau.

1. Introduction

River transport is the main process controlling fluxes of most elements from continents to oceans (Garrels & Mackenzie, 1971; Gaillardet et al., 2003). The marine isotope and element inventory is thus strongly dependent on continental weathering processes and subsequent river transport to the ocean basins. In the case of the highly redox sensitive molybdenum (Mo), the continental contribution accounts for the predominant part of the marine Mo budget (Morford &

Emerson, 1999; McManus et al., 2002, 2006). Once dissolved Mo has entered the oceans, redox-dependent isotope fractionation accompanies its incorporation into sediments, covering all environments from oxic to strongly euxinic. As each of these environments shows characteristic isotope signatures (Barling et al., 2001; Barling & Anbar, 2004; Siebert et al., 2003, 2006; Neubert et al., 2008), Mo isotopes in marine sediments have been used to investigate the evolution of atmospheric O_2 and to quantify the extent of seafloor anoxia in the geological record (e.g., Arnold et al., 2004; Siebert et al., 2005; Wille et al., 2007; Pearce et al., 2008; Voegelin et al., 2010). All of these models rely upon the assumption of a fairly uniform long-term riverine Mo isotope input signature of around 0‰ based on the available $\delta^{98/95}$Mo data of crustal igneous rocks (-0.1 to +0.3‰; Siebert et al., 2003). Arnold et al. (2004) additionally included continental molybdenites (average of -0.1‰, Barling et al., 2001) in their model. Recent publications by Archer & Vance (2008), Pearce et al. (2010) and Neubert et al. (2011), however, have revealed not only a preferential enrichment of river waters in the heavy isotopes but also a large variability of their $\delta^{98/95}$Mo signature (-0.13 to 2.3‰). The pronounced discrepancy between the assumed crustal background and the aquatic signature thus emphasizes the need for a more thorough investigation of isotope fractionation processes during chemical rock weathering in the terrestrial environment.

The heavy Mo isotopic composition of sedimentary source rocks was found to be reflected in the associated river water $\delta^{98/95}$Mo, suggesting a predominant control of catchment outcrop weathering (Neubert et al., 2011). Thereby, sulfate weathering and sulfide oxidation were proposed to play a crucial role in liberating Mo from the different source rock types. Leach experiments performed by Liermann et al. (2011) on black shales document an enrichment of the solution in heavy Mo isotopes. The offset between the starting material and the leach

solutions was interpreted to be caused by adsorption of dissolved Mo to Fe- and Mn-(oxyhydr)oxides, as they preferentially adsorb light Mo (Barling et al., 2001; Siebert et al., 2003; Goldberg et al., 2009). An analogous process, i.e. adsorption of Mo onto the suspended load during river transport, was suggested as a potential removal process of light Mo in natural environments (Archer & Vance, 2008; Pearce et al., 2010). Finally, the same authors proposed that soil retention of light Mo is an important process to control river water Mo.

This study investigates Mo isotope fractionation processes during weathering of crustal igenous rocks (basalt, granite, orthogneiss) in a small catchment basin located in the French Massif Central. Although weathering of magmatic rocks has in the past not been associated with significant Mo isotope fractionation due to their small $\delta^{98/95}$Mo variability, stream waters analyzed here are enriched in the heavy isotopes. In order to identify the role of various Mo sources and weathering processes, stream water and bedrock data were complemented by measurements of the suspended load, soil material and vegetation. The Mo data of natural samples were compared to results of successive bulk rock leaching experiments. These experiments were conducted on all three bedrock lithologies in order to simulate the weathering behavior of different crustal igneous rock types and their role in generating the observed heavy aquatic $\delta^{98/95}$Mo signals. Special emphasis was thereby placed on the effect of mineral dissolution and adsorption effects. To identify the Mo hosting phases and to constrain mass balance, laser ablation ICP-MS was used to obtain element concentrations of single mineral grains and sulfidic melt inclusions.

2. Study site and sampling

2.1. Geological setting

The mixed basaltic-granitic catchment basin is located in the southern part of the French Massif Central (Fig. 1). It covers an area of around 68 km^2 and includes two streams, the Séjallières and the Malaval. The eastern and most elevated part (1301 m a. s. l.) is formed by Quaternary basalts. Downstream and to the west the catchment basin drops to an altitude of 714 m a. s. l. and is characterized by deep and narrow valleys with Hercynian granitic and orthogneissic bedrock. Due to its low inclination, the basalt plateau is covered by well developed soils and swampy areas. The steep orthogneissic and granitic hillsides to the west are covered by forests and exhibit a poorly developed soil cover.

2.2. Sampling

Stream water was collected during two field campaigns in June 2003 (see Steinmann & Stille, 2008) and June 2010. Sampling locations are shown in Fig. 1 and listed with respect to their upstream distances from the catchment outlet in Table 1. All waters were filtered on site using 0.45μm nylon filters and Nalgene™ filtering units. Subsequently, they were acidified with distilled nitric acid and stored in pre-cleaned LDPE bottles for isotope and trace element analysis. Anion determinations were done on filtered, non-acidified aliquots. Filters were dried and weighed prior to and after water sampling in order to determine the suspended load for each filter. Basaltic bedrock samples were collected in the riverbed of the study area. Additional basalt material was collected in a quarry located north of the catchment outlet (Fig. 1) as these rocks were particularly fresh. Well preserved granite and orthogneiss samples were collected during earlier fieldwork. One soil sample was taken in a swampy

area on the basalt plateau. A soil sampler was used to recover the topmost ca. 30 cm. In the lab, root material for Mo analyses was extracted from the soil.

2.3. Rock sample descriptions

Basalt sample PA-1 is a fine grained olivine basalt, containing medium sized phenocrysts of olivine and clinopyroxene and small phenocrysts of plagioclase, embedded in a dense microcrystalline matrix. The opaque phases are predominantly titanomagnetites. Opaque sulfidic melt inclusions occur as small ($<30\mu$m) droplets as identified in silicate phenocrysts. Basalt M29-R is mineralogically identical with smaller olivine, pyroxene and plagioclase phenocrysts when compared to sample PA-1. The biotite rich orthogneiss (AR-7) has a medium to coarse grained texture. It is composed of quartz, potassium feldspar and plagioclase and contains only few oxides and sulfides. The fine grained granite (LC-1) is dominated by quartz, potassium feldspar, biotite, plagioclase and contains some muscovite. Apatite and zircon occur as accessory phases and oxides and sulfides are rare.

3. Analytical methods

3.1. Leach experiments

In order to investigate the behavior of Mo isotopes during progressive rock weathering, rock samples were exposed to acid leach experiments under oxidizing conditions using 0.3 and 2 mol L^{-1} HCl and HNO_3. The experiments were performed at low pH ($\leq$1) to preclude secondary mineral formation (Pistiner & Henderson, 2003) and adsorption related Mo isotope fractionation (see section 5.2.3). These conditions should insure that the impact of primary mineral dissolution on the leach solution $\delta^{98/95}$Mo is isolated.

Experiments were conducted on both basalt grains and powders, and orthogneiss and granite powders. Samples were prepared by cutting off sections

affected by rock weathering. Subsequently, slabs were crushed in a hydraulic press. Grains of 0.1-0.5 mm in size were separated, sonicated and rinsed repeatedly with high purity H_2O (>18.2 M Ωcm^{-1}). Powders were ground in an agate ball mill, and multiple aliquots were processed to determine representative bulk rock $\delta^{98/95}$Mo compositions and concentrations for all rocks. All sample splits were weighed into screw-top PTFE beakers prior to leaching. Up to eight grams of basalt grains were immersed in 50 ml 0.3 mol L^{-1} HNO_3 and 0.3 mol L^{-1} HCl at room temperature for a period between 10 minutes and 2 months. Powder samples were processed using 0.3 mol L^{-1} HNO_3 at room temperature and 2 mol L^{-1} HNO_3 at a constant temperature of 50 °C. Periods of between 2 minutes and 7 days were chosen for these experiments. This setup produced leach solutions with a considerable range of fractional Mo release. Due to the overall low Mo content, particularly of the orthogneiss and granite (<0.4 μg g^{-1}), each leach experiment was performed on an individual sample split. Separation of acid solutions from rock materials was done by centrifugation and subsequent filtering through 0.2 μm nylon syringe filters. Finally, the Mo isotopic compositions and concentrations of leach solutions as well as selected residues were analyzed.

3.2. Preparation of water, rock, soil and vegetation samples

Prior to any sample processing and chemical Mo purification procedures a double spike with masses ^{100}Mo + ^{97}Mo (see Siebert et al., 2001 for details) was added to all sample types in order to account for any potential Mo isotope fractionation during column chemistry (Anbar et al., 2001; Siebert et al., 2001) and to correct for instrumental mass bias during measurement. Double (HF) and triple (HCl and HNO_3) distilled acids and 30% suprapure hydrogen peroxide were used for all digestion and purification steps. Powdered bulk rock samples were treated with concentrated HCl + H_2O_2 and HF + HNO_3 dissolution steps

to ensure complete digestion of the silicate matrix (Siebert et al., 2001; Wille et al., 2007). Soil material was dried at 60°C and subsequently sieved to separate it from rock pebbles and root material. Roots were cleaned in an ultrasonic bath and rinsed repeatedly with high purity H_2O to remove any residual soil particles. Soil and root samples were digested using multiple HNO_3 and HF steps closely following the procedure described in Cenki-Tok et al. (2009). Between 0.5 and 2 liters of filtered stream water were evaporated prior to column chemistry.

3.3. Chemical purification and isotope analysis of Mo and Sr

Mo was purified from all samples using an anion exchange column (1 mL Dowex 1X8 resin, 200-400 mesh). A cation exchange column (2 mL Dowex 50WX8 resin, 200-400 mesh) was used additionally to remove any residual iron (procedure after Siebert et al., 2001 and Wille et al., 2007). For Sr purification, eluted matrix solutions, obtained from Mo anion column separation, were evaporated and loaded onto Sr Spec™ columns. For MC-ICP-MS measurements, the evaporated Mo and Sr fractions were re-dissolved in 0.5 mol L^{-1} HNO_3. Mo isotopic compositions and concentrations as well as Sr isotopic compositions were measured at the University of Bern on a double-focusing ®Nu-Instruments MC-ICP-MS connected to an Apex™ desolvating nebulizer. The Mo isotopic composition is measured relative to a standard solution (Johnson Matthey, 1000μg mL^{-1} ($\pm$0.3%) ICP standard solution, lot 602332B). This standard is 2.3‰ below modern open ocean seawater (Siebert et al., 2003). Final Mo isotopic data are reported as $\delta^{98/95}$Mo=[(^{98}Mo/^{95}Mo)$_{Sample}$/(^{98}Mo/^{95}Mo)$_{Standard}$-1]$\times$ 10^3. The data presented were acquired with a preferred quantity of >60 ng and a minimum of 30 ng of Mo in solution. Total chemistry Mo blank was <1 ng. The external standard reproducibility of the $\delta^{98/95}$Mo ratio is $\pm$0.1% at the 2σ level (Siebert et al., 2003). For Sr isotope analyses the samples were diluted down to an optimum amount of 50 to 100 ng. The external reproducibil-

ity of the NIST SRM 987 standard during the period of the present analyses was 0.710235±0.000029 (2σ). The external reproducibility of of the NIST SRM 987 standard measured by Steinmann & Stille (2008) was at 0.710259±0.000016 (2σ).

3.4. Major anion and cation analyses of stream waters and leach solutions

Major anion and cation contents of all river water samples (except M31-Ft and M31-Fu) were determined on 0.22μm filtered sample fractions at the laboratory of Chrono-Environnement, CNRS / University of Franche-Comté, Besançon (France). Na^+, K^+, Ca^{2+} and Mg^+ were analyzed with a Perkin Elmer A Analyst 100 atomic absorption spectrometer (AAS) on sample aliquots acidified with HNO_3 to pH 2 after filtering. F^-, Cl^-, NO_3^- and SO_4^{2-} were measured with a Dionex DX100 high-pressure ion chromatograph on unacidified sample aliquots. HCO_3^- concentrations were determined in the field within a few hours after sampling (in order to limit exchange with atmospheric CO_2) on unfiltered and unacidified samples by standard titrimetric methods considering total and carbonate alkalinity as equivalent and equal to HCO_3^-. Typical uncertainties including all error sources for major cations, anions and alkalinity lie between ±4 % and ±6 %, depending on the concentration levels (Steinmann & Stille, 2008; Binet et al., 2009). Major anion and cation concentrations of river water samples M31-Ft and M31-Fu as well as SO_4^{2-} concentrations of the leach solutions were determined using a Metrohm®861 Advanced Compact Ion Chromatograph at the University of Bern.

3.5. Laser ablation ICP-MS analyses of bedrock minerals

LA-ICP-MS analyses were performed on silicate phenocrysts, oxides, sulfide melt inclusions (entirely enclosed in the host mineral) and the fine grained matrix of basalt sample PA-1. Measurements were performed on a GeoLas-Pro 193

nm ArF excimer laser system in combination with a Perkin Elmer Elan DRC-e quadrupole mass spectrometer at the University of Bern. Instrumental conditions were similar to those reported in Pettke (2008). Major and trace element concentrations were measured using spot sizes between 16 and 120 μm, with the 120 μm beam used for bulk matrix compositions. Bracketing standardization using SRM 610 from NIST was used for instrument sensitivity calibration and drift correction. The standard contains sixty-one trace elements doped in a Si-Na-Ca-Al matrix, most of which are homogeneously distributed (Eggins & Shelley, 2002). Data quantification used the SILLS software package (Guillong et al., 2008), employing the major element oxide total of 100 wt% for internal standardization. For sulfide melt inclusions, data were treated following Halter et al. (2002). The mixed inclusion plus host mineral signal was deconvolved by assuming that no SiO_2 is present in the sulfide melt inclusion; hence, the Mo concentrations obtained are those present in the pure sulfide inclusion.

4. Results

4.1. Natural samples

4.1.1. Stream water and bedrock geochemistry

All stream water Mo data are given in Table 1 and shown in Fig. 2. Overall, the waters show a moderate $\delta^{98/95}$Mo variability between 0.55 and 1.1 ‰. The waters of both streams sampled in 2003 show a tendency towards slightly higher $\delta^{98/95}$Mo values. Mo concentrations were also higher in 2003 (0.17-0.81 ng g^{-1}) than in 2010 (0.02-0.15 ng g^{-1}). Field parameters and further chemical compositions of the stream waters are listed in Table 2.

Analyses performed on multiple splits of all three igneous rock types (Table 3) reveal different signatures ranging from a minimum of -0.28 ‰, detected in an orthogneiss split (median $\delta^{98/95}$Mo=-0.2 ‰, n=7), to a maximum of 0.70 ‰

(median $\delta^{98/95}$Mo=0.58 ‰, n=5) in the granite. By contrast, the two basalts PA-1 and M29-R show median $\delta^{98/95}$Mo values of 0.14 (n=6) and 0.07 ‰ (n=5), respectively. Hence, the basalts are the only igneous bedrock to comply with the Mo isotope signature of the basalts and granites measured by Siebert et al. (2003) ($\delta^{98/95}$Mo = -0.1 to 0.3 ‰). The three different bedrocks exhibit strongly variable Mo concentrations, with median values of 0.08 μg g^{-1} and 0.33 μg g^{-1} for the orthogneiss and the granite. The basalts show median Mo concentrations of 3.5 μg g^{-1} (PA-1) and 2.4 μg g^{-1} (M29-R). Two basalt sample splits reached Mo concentrations as high as 7.7 and 4.8 μg g^{-1}, indicating a nugget effect on bulk rock Mo concentrations. The concentrations measured in this study are more variable compared to the assumed upper crust value of 0.78-1.5 μg g^{-1} (Rudnick & Gao, 2004, and references therein).

Bedrock Sr isotope data are taken from Steinmann & Stille (2008). Table 3 lists values typical for the individual rock types. A pronounced difference exists between the high ^{87}Sr/^{86}Sr ratios of orthogneiss and granite (typically between 0.720-0.750) and the low ratios of the basalt (ca. 0.703). The stream waters show the ^{87}Sr/^{86}Sr ratio typical of basalt on the plateau and a smalll increase of the ^{87}Sr/^{86}Sr ratio downstream (Table 1), reflecting the contribution of gneiss and granite.

4.2. Single grain and matrix element concentrations determined by LA-ICP-MS

Element concentrations of single minerals and the basalt matrix (averages) are given in Table 4, data of sulfidic melt inclusions in Table 5. The silicate phenocrysts have Mo concentrations reaching 0.1 to 0.2 μg g^{-1} in olivine and pyroxene, and between 1 and 2 μg g^{-1} in plagioclase. The Fe-Ti oxides contain between 0.5 and 1.2 μg g^{-1} Mo. The fine grained basalt matrix has an average Mo concentration of 3.5 μg g^{-1} with minimum values at 2.7 μg g^{-1} and a maximum at 5.5 μg g^{-1}. The sulfide melt inclusions have strongly variable Mo

contents ranging from values $<0.05 \mu g\ g^{-1}$ to as high as 250 $\mu g\ g^{-1}$. According to their Fe, Cu and Ni concentrations they can be subdivided into three different inclusion types. Type 1 has high Fe/Cu and Ni/Cu ratios and Mo concentrations $<2\ \mu g\ g^{-1}$, type 2 exhibits moderate Fe/Cu and Ni/Cu ratios and very variable Mo concentrations between 0.3 and 250 $\mu g\ g^{-1}$, type 3 shows very low Fe/Cu and Ni/Cu ratios and intermediate Mo concentrations between 16 and 80 $\mu g\ g^{-1}$.

4.3. Soil, vegetation and suspended load

The soil sample, as well as root material extracted from it, show moderately negative $\delta^{98/95}$Mo values of -0.33 and -0.14 ‰ (Table 6). A concentration of 0.67 $\mu g\ g^{-1}$ was found in the roots, the soil is more enriched with a concentration of 2.4 $\mu g\ g^{-1}$. Data of the suspended load are given in Table 7. The amount of suspended load lies between 1.3 and 19.7 mg L^{-1} in the 2003 samples, while in 2010 the suspension weight was below detectable limits by weighing. Also, most of the suspended load samples taken in 2010 had Mo concentrations not exceeding Mo blank levels (<1 ng). Due to the low amount of suspended load in 2010, no Mo isotope composition and concentrations could be determined. Samples taken in 2003 were not available for measurement.

4.4. Laboratory leach experiments

4.4.1. Basalt leach solutions and residues

Data of all leach solutions and residues are listed in Table 8. Experiments performed on grains of sample PA-1 show identical leach solution $\delta^{98/95}$Mo values for both the HCl and the HNO_3 leach (Fig. 4), all of which are isotopically significantly heavier than the starting material. Mo isotopic compositions lie between 0.61 and 0.84 ‰ with up to 9 % of the total rock Mo inventory extracted. Powder leach solutions of the same basalt reveal a similarly narrow range of Mo isotopic compositions (0.42-0.88 ‰). In these experiments, up to

54 % of the total bedrock Mo were released (Fig. 4). Leaching of basalt M29-R liberated up to around 30 % of Mo and shows solution $\delta^{98/95}$Mo signals consistent with those of PA-1 (0.53-0.97 ‰; Fig. 5). The evolution of the Mo isotope ratio as a function of increased leach fractions is nearly identical for both basalt samples. Between the initial, extremely rapid Mo release and Mo extraction of 30 %, no significant trend appears in the $\delta^{98/95}$Mo signal of PA-1. Only at a Mo release of approximately 54 % Mo the $\delta^{98/95}$Mo decreases. In the leach series of sample M29-R, the isotope compositions are slightly higher at lower leach fractions ($\leq$ 15%) and decrease at higher fractions. Leach residues of PA-1 experiments show a broad range of $\delta^{98/95}$Mo values from 0.12 to -0.29 ‰ (Fig. 4). The lowest values were observed at the longest leach times, corresponding to the highest proportion of extracted heavy Mo.

The different leach setups produced different Mo release patterns (Fig. 6A). HCl and HNO_3 grain leach solutions show increasing concentrations reaching a maximum of 0.3 μg g^{-1}. After a rapid initial Mo release the leaching rate slowed. The largest Mo release occured during the 2 mol L^{-1} HNO_3 powder experiments where maximum Mo concentrations of 1.9 μg g^{-1} (PA-1) and 0.7 μg g^{-1} (M29-R) were extracted from the basalts. The interaction between basalt powders and 0.3 mol L^{-1} HNO_3 produced solutions with considerably lower Mo concentrations (0.2-0.4 μg g^{-1}). Also, a quick initial Mo release is followed by a concentration decrease with time. Sulfate concentrations of leach solutions increased with time, correlating with increasing Mo concentrations (R^2=0.9 linear correlation; Fig. 6B).

4.4.2. Orthogneiss and Granite leach solutions

Powder leach experiments performed on the orthogneiss (AR-7) extracted between 1 and ca. 100% of the bedrock Mo inventory (Table 8, Fig. 5C). The isotopic compositions of the leach solutions vary between 0.11 ‰ and -0.15 ‰.

Leach rates for the granite (LC-1) are much lower since only approximately 1-8 % of the total Mo were released applying the same leach times. Showing values between 1.03 and 1.38 ‰, the granite leach solutions are isotopically much heavier than those of the orthogneiss (Fig. 5A).

5. Discussion

5.1. Natural samples: bedrock and stream waters

The catchment morphology promotes the formation of well developed weathering profiles on the plateau and hampers rock-water interaction in the steep granitic and orthogneissic hillsides. As a consequence, the mafic rocks, highly susceptible to weathering processes (Gislason & Eugster, 1987), are favored as the primary lithological control on the stream water geochemistry. Their predominance is shown by the aquatic Nd and Sr isotope data of Steinmann & Stille (2008) and Sr data of this study (Table 1), which mainly reflect the signature of the basalt; the contribution from granites and orthogneisses is subordinate. Data collected on all three riverbed rock types indicate an analogous basalt dominance for the river dissolved Mo system as the median Mo concentration of the mafic rocks of 2.4 and 3.5 μg g^{-1} is about one order of magnitude higher than that of the felsic bedrock types (<0.4 μg g^{-1}; Fig. 3). However, unlike the Sr and Nd isotope signatures, the $\delta^{98/95}$Mo of both the Malaval and the Séjallières do not concur with the isotopic composition of the basalt but are enriched in the heavy isotopes. With a median value of 0.58 ‰ the granite is isotopically slightly heavier than the previously reported magmatic rocks by Siebert et al. (2003) and represents the only rock type with a $\delta^{98/95}$Mo signature approximating that of the stream waters. Yet the granite cannot account for the isotopically heavy waters of the Séjallières, as it is crosscut only by the Malaval. The orthogneiss potentially contributes Mo to both the Séjallières and the lower segment of the

Malaval. Nevertheless, the extremely low concentrations (median=0.08 μg g^{-1}, n=7) exclude the orthogneiss from being an important contributor to the overall aquatic Mo budget. The moderate stream water $\delta^{98/95}$Mo variations do not coincide with the sampling distance from the catchment outlet (Fig. 2). The lack of any systematic $\delta^{98/95}$Mo downstream trend of the river dissolved load, despite changing environmental conditions (i.e. bedrock type, soil cover, topography), as well as the overall small variability of the aquatic Mo signature may further support the idea of a single dominant source rock. The waters of both streams sampled in 2003 show a tendency to slightly higher $\delta^{98/95}$Mo values and a greater variability (0.7-1.1 ‰) than in 2010 (0.6-0.9 ‰). This marginal isotopic shift coincides with an increase in the amount of suspended particles, which was generally higher in 2003 than in 2010 (Table 7). Mo isotope fractionation through adsorption of Mo to (oxyhydr-)oxide particles (Barling & Anbar, 2004; Goldberg et al., 2009) might thus be considered a process contributing to the isotopic composition of the river dissolved load. This process was previously proposed to cause the suspended load to be isotopically lighter than the dissolved load (Pearce et al., 2010), in return increasing the stream water $\delta^{98/95}$Mo values. While this may explain the small difference in $\delta^{98/95}$Mo between 2003 and 2010, it cannot account for the 0.5 to 1 ‰ offset between the basalt bedrock and the stream waters. Even in 2010, when the amount of suspended load is negligible, a large $\delta^{98/95}$Mo offset exists between the bedrock and the river dissolved load.

5.2. Experimental primary mineral dissolution

5.2.1. Incongruent bedrock weathering

Mild acid leach experiments performed by Siebert et al. (2003) on granite did not generate a heavy dissolved Mo pool, but released Mo with a $\delta^{98/95}$Mo composition indistinguishable from that of the crustal starting material. These

data have consequently been used to assume that igneous crustal rock weathering has no importance in producing the heavy $\delta^{98/95}$Mo of river waters (e.g., Nägler et al., 2005; Pearce et al., 2010). In contrast to the data of Siebert et al. (2003), the basalt and granite leach solutions produced in the present study are not identical to the $\delta^{98/95}$Mo compositions of the bulk rock but show a considerable enrichment in the heavy isotopes (Figs. 4 and 5 A & B). In contrast, Mo freed from the orthogneiss matrix is only very weakly fractionated when compared to the starting material (Fig. 5C). These results indicate that the isotopic composition of Mo released during the partial dissolution of igneous rocks is dependent on the bedrock mineralogy. Accordingly, the weathering of igneous crustal rocks is incongruent and likely controls the river dissolved Mo signature. In fact, the striking consistency between the $\delta^{98/95}$Mo of the basalt leach solutions (0.5 to 1 ‰; Figs. 4 and 5B) and that of the stream waters (0.6 to 1.1 ‰; Fig. 2) strongly suggests that the $\delta^{98/95}$Mo in these streams is controlled by bedrock weathering. Furthermore, it corroborates the interpretation that basalt is the single most important source contributing to the stream water Mo geochemistry in the catchment investigated here. Consequently, Mo host phases and their respective importance for mass balance need to be constrained.

5.2.2. Mo released from basalts: host phases and mass balance

The interpretation of the basalt leach patterns (Figs. 4 and 5B) requires knowing the Mo content of the individual rock components. This permits the performance of mass balance calculations to identify the relevant Mo host phases. The discussion focuses on basalt PA-1 (Fig. 4), as the larger sized phenocrysts facilitate a precise determination of Mo concentrations of individual components by LA-ICP-MS. Note, that although the two basalts have identical mineralogical compositions and their leach solutions show the same $\delta^{98/95}$Mo variability, the modal abundance of the individual rock components may vary

between samples M29-R and PA-1. This is expressed by the difference in the fraction of Mo released at identical leach times (2 mol L^{-1} HNO_3 leach: 20-30% in M29-R and 30-55% in PA-1; Table 4).

The Mo distribution among the different rock components is fairly heterogeneous. Thereby, moderately to strongly enriched phases can be distinguished from depleted phases (Tables 4 and 5). Also, while the Mo content of the sulfide melt inclusions is highly diverse, all other rock constituents show minor Mo variability. Mass balance calculations indicate that when combined, the low concentration oxides and silicate phenocrysts only account for a minor fraction of the total Mo rock inventory (3-4 %; Table 4) and, hence, their role in producing the leach patterns is irrelevant. The Mo content of basalts is intimately connected to how evolved the parent basalt magma is (Arnórsson & Oskarsson, 2007; Audétat, 2010). Therefore, the offset between the generally depleted silicate phenocrysts and the moderately enriched silicate matrix is attributed to fractional crystallization, which results in a progressive Mo enrichment of the magma (Audétat, 2010). Accordingly, the depleted phenocrysts are likely to record the composition of the early magma, while the matrix represents the evolved, residual melt, where Mo accumulated due to its incompatibility. The three types of sulfide melt inclusions (Table 5) reflect different stages of silicate melt evolution because of their magmatic equilibrium coexistence. They show distinct Mo concentration patterns with each stage, finally resulting in the pronounced Mo variability.

Due to the low Mo concentrations of silicate phenocrysts and oxides, the sulfide phases and the matrix remain primary sources of Mo and, hence, dominate the Mo budget of the solution. It has been argued previously that sulfide dissolution is an important weathering process, very likely to generate distinguishable geochemical patterns of the riverine dissolved load (Neubert et al., 2011). The

elevated Mo contents found in some of the melt inclusions and the rapid progression of sulfide weathering in oxygenated environments (Anbar et al., 2007) here leads to the hypothesis that the preferential dissolution of the magmatic sulfides causes the isotopically heavy Mo in the basalt leachates. Increasing SO_4^{2-} concentrations, which go along with heavy $\delta^{98/95}$Mo and increasing Mo concentrations of the liquid phase (Fig. 6A), support this interpretation. If the sulfides are the primary and most readily dissolved Mo source, then the isotopic composition of the leachates would require them to host at least 25 to 30 % of the total bedrock Mo (Fig. 4) despite being rare (<1 % modal abundance). Mass balance calculations are therefore used to check whether the experimentally derived data can be explained by the sulfides alone. Within the limits set by the geochemical and optical data (Tables 4 and 5) the system shows a very high sensitivity to changes of both sulfide concentration and abundance. Changing these parameters for all other components has a much smaller effect. The calculations presented in Table 9 are thus based on constant, representative values for silicate phenocrysts, oxides and the matrix. By changing the sulfide parameters, the entire range of experimentally released heavy dissolved Mo can be reproduced. These data demonstrate that even few magmatic sulfide grains can account for a large fraction of the total bedrock Mo inventory. As leaching progresses the contribution from other rock components becomes progressively more important. Supporting evidence is given by the significant $\delta^{98/95}$Mo drop observed in the residues at leach amounts >30 %, suggesting that the heavy sulfide reservoir is exhausted and that the influence of an isotopically lighter component increases. This component is most likely the matrix, since it accounts for the largest fraction of the bulk rock Mo inventory associated with preferentially weathered devitrified glass. Gradual admixture of isotopically lighter matrix-derived Mo also explains the lowered $\delta^{98/95}$Mo of the solution at

a leach amount of 54 % ($\delta^{98/95}$Mo = 0.42 ‰, Fig. 4).

On its own, the experimental data (Figure 4) could theoretically be reconciled with equilibrium fractionation. In the context of all available information (sulfate and LA-ICPMS data as well as mass balance calculations), however, the proposed model is the most likely. A simple two-component model (solid-liquid) does not realistically describe the data, as we are dealing with a three-component system (solution-sulfides-silicate matrix). Finally, sulfide is identified as the source of heavy $\delta^{98/95}$Mo due to the correlation with sulfate (R^2=0.9 linear corrleation; Fig. 6B).

These data strongly suggest that Mo isotopes are fractionated between coexisting silicate and sulfide melts in basaltic systems, with sulfide melt being isotopically heavier than silicate melt. Therefore, the results indicate that Mo isotope fractionation is likely to occur at hot magmatic conditions. Iron isotope fractionation of similar magnitude has previously been observed at magmatic temperatures between sulfide (phyrrotite) and silicate melt (Schuessler et al., 2007) as well as between silicate (fayalite) and magnetite (Shahar et al., 2008). It remains to be established whether the observed Mo isotope fractionation is primarily due to crystallographic control of phases involved in such processes or is rather a consequence of changing intensive properties such as density.

5.2.3. The role of Mo adsorption to Fe-Ti oxide surfaces during experimental dissolution

As mentioned earlier, the low pH of the leaching agents should prevent secondary mineral formation during the experiments (Pistiner & Henderson, 2003) and isolate Mo isotope fractionation related to primary mineral dissolution. In particular, Fe^{3+} does not precipitate and form additional phases (Johnson et al., 2004). Mo adsorption to metal (oxyhydr)oxide surfaces, however, is increased under these conditions (e.g., Goldberg et al., 1996; Xu et al., 2006; Kim & Jang,

2010) and thus Mo adsorption to the preexisting titanomagnetite surfaces may have caused Mo isotope fractionation unrelated to mineral dissolution. Since Mo adsorption to Fe-Mn (oxyhydr)oxide surfaces preferably removes the light isotopes from solution (Siebert et al., 2003; Barling & Anbar, 2004; Goldberg et al., 2009), the observed isotope fractionation (Δ^{98}Mo) between leach solutions and basalt could potentially be attributed to adsorption rather than to the dissolution of specific bedrock minerals. Assuming that the experimentally determined fractionation factor between magnetite and the dissolved phase (Δ^{98}Mo=0.83 $\pm$0.6 ‰; Goldberg et al., 2009) is applicable to Ti bearing magnetite as well, the predicted basalt-leachate isotope fractionation agrees with the isotope fractionation between solid and solution observed in this study (Δ^{98}Mo=0.4-0.9). However, fractionation factors of Goldberg et al. (2009) were determined at high pH (6.9-8) with Mo present as the tetrahedrally coordinated MoO_4^{2-}. At the low pH, at which the experiments of this study were conducted ($\leq$1), Mo is exclusively present in the octahedral form (Cruywagen & Heyns, 1989, 2000; Ozeki et al., 1996). Since fractionation of Mo isotopes during adsorption to (oxyhydr)oxide surfaces occurs dominantly as a result of the transition from the tetrahedrally to the octahedrally coordinated Mo species (Tossel, 2005; Goldberg et al., 2009), the fractionation factor between solid and solution decreases with more acidic pH, i.e. high proportions of octahedral Mo in solution. Consequently, Δ^{98}Mo is expected to be strongly reduced in the present experiments and the observed large fractionation cannot be attributed to adsorption onto the Fe-Ti oxide surfaces. This prediction is supported by the Mo concentration as well as isotope data. First, although the decreasing Mo contents observed in the 0.3 mol L^{-1} powder experiments is compatible with adsorption, no concomitant change in $\delta^{98/95}$Mo occurs (Fig. 4). Secondly, the increasing Mo concentrations observed in all other experiments suggest that adsorption is not significant. Fi-

nally, in a two phase closed system equilibrium process exhibiting a constant fractionation factor, as it is the case in the experiments here, any liquid will show increased $\delta^{98/95}$Mo values with increasing Mo adsorption. The $\delta^{98/95}$Mo of the leach solutions, however, show no such trend (Fig. 4). Hence, the observed large isotope fractionation cannot be attributed to adsorption onto the Fe-Ti oxide surfaces. The discrepancy between the concentration data of the 0.3 mol L^{-1} and the 2 mol L^{-1} leaches (decreasing vs. increasing Mo concentrations, Fig. 6B) may conceivably be a function of variable pH. Adsorption reaches a maximum between pH 2 and 4 (Goldberg et al., 1996) and the subsequent implied decrease could gradually limit adsorption at pH $\leq$2, resulting in the differing concentration patterns of the leachates.

5.3. Implications for the natural environment

The interpretation of the leach patterns indicates that incongruent phase dissolution of bulk rocks in general, and fast magmatic sulfide dissolution in particular, greatly influences how Mo isotopes are disproportionated during crustal bedrock weathering. With respect to the natural environment, the close match between the $\delta^{98/95}$Mo signatures of stream waters and experimental leach solutions suggests that the dissolution of isotopically heavy magmatic sulfides during basalt outcrop weathering is likely to be the key factor in producing the aquatic signatures of the Malaval and the Séjallières. These results raise important questions pertaining to the relevance of soil formation and adsorption processes, which have been considered vital in producing heavy river water $\delta^{98/95}$Mo signatures (Archer & Vance, 2008; Pearce et al., 2010). According to the combined results of leach solutions and stream waters, soil formation and adsorption appear to have a minor effect on the isotopic signature of the dissolved Mo in the catchment basin under investigation. However, the soil sampled on the plateau exhibits a negative $\delta^{98/95}$Mo, typically produced by Mo adsorption

to Fe-Mn (oxyhydr)oxides. Even so, this is most probably not the primary process causing the two streams to be enriched in the heavy Mo isotopes, and based on the experimental data an alternative process is proposed here. Incongruent chemical basalt weathering preferentially releases isotopically heavy magmatic sulfide Mo that dominates the dissolved Mo inventory. In the case of the Malaval and the Séjallières, the extraction of sulfide-bound Mo within the regolith cover is reflected in the aquatic sulfate concentrations, which are elevated in the lower parts of the catchment where streams are affected by regolith-derived waters (Table 2). Similarly, other stream water parameters also show an enrichment in the lower regions. This effect may be additionally amplified by rain water admixture to the surface waters on the plateau, because precipitation is generally depleted in Mo (e.g., Kawakubo et al., 2001).

The isotopically heavy Mo of river waters is most likely the result of a complex interplay between various processes involved, and the mass balance between the competing factors likely controls the aquatic $\delta^{98/95}$Mo. The local system is highly dependent on rock mineralogy, degree of rock weathering and soil development, secondary mineral precipitation and the availability of mineral surfaces for adsorption. In the case presented here, magmatic sulfide mineral dissolution within the basaltic riverbed and regolith appears to dominate all other processes. Finally, future studies will not only have to focus on Mo isotope fractionation during mineral dissolution and soil formation, but also on the importance of vegetation in the terrestrial Mo cycle, because the role of Mo as an essential micronutrient required by plants is well known (e.g., Mendel & Bittner, 2006; Fitzpatrick et al., 2008). The root and soil Mo isotope and concentration data presented here indicate that Mo uptake into the biomass is considerable and, therefore, may be an important additional pathway for the removal isotopically light Mo in the weathering environment.

5.4. Consequences for the global Mo isotope budget

The observation that most Mo isotopic compositions of dissolved river loads are heavier than most of the silicate magmatic rocks analysed so far raises two related problems. Firstly, the fate of the light Mo isotopes missing in the balance needs to be evaluated; secondly, the effect of isotopically heavy river water on the constancy of the continental input needs to be quantified. Different explanations for the heavy Mo isotopic composition of river waters have been put forward. Archer & Vance (2008) proposed retention of light Mo isotopes in soils, while Neubert et al. (2011) proposed the Mo isotopic composition of catchment source rocks as the predominant control on the dissolved riverine $\delta^{98/95}$Mo, stressing that sedimentary rocks (especially marine carbonates and sulfates) have a different $\delta^{98/95}$Mo from the magmatic silicates. The hypothesis of incongruent rock weathering presented in this paper is not meant to be a substitute for the former explanation, but rather a complementary process. The relative effect of the processes that affect the Mo isotopic composition of rivers on the global Mo isotopic cycle depends on the time scale. On a global scale, the total volume of soil (or weathered rock volume) at any given time is limited. If light Mo isotopes are preferentially retained in soil and/or weathering residues, erosion will liberate them sooner or later. When the integrated volume of soil formation is equal to the integrated soil erosion, the net Mo isotope effect will be zero. This is certainly true for very long time-scales. Likewise, whenever the globally integrated incongruent weathering of (sulfide bearing) fresh rocks is balanced by erosion of already weathered rocks, the Mo isotope effect will also be zero. The fact that to date there are no reports of magmatic rocks with a particularly low $\delta^{98/95}$Mo (i.e. residues of intense sulfide weathering) may well be related to an intentional sampling bias: to constrain the magmatic Mo isotopic composition of such rocks, fresh samples were collected and measured,

not highly weathered ones. The only way to bias the total continental runoff towards an isotopic composition heavier than the continental crust (magmatic plus sedimentary rocks) requires a continuous net increase of the volume of soils and weathered rocks on a global scale, which, however, is not a long-term steady state that can be maintained over geological times. On the other hand, the hypothesis that the $\delta^{98/95}$Mo of catchment rocks accounts for the heavy Mo isotopic composition of river water is independent of the need to achieve a steady state. It applies to the whole geological period, for which marine sediments exposed to subaerial erosion show a heavy $\delta^{98/95}$Mo signature; basically this includes post Archean times.

Even if soil processes and incongruent weathering are transient, there is ample possibility that they do influence the Mo isotopic composition of the continental runoff in selected periods of Earth's history, namely when the Earth system was exceptionally far from steady state. Amongst the conceivable examples are large subaerial basaltic eruptions (LIPs: e.g., Deccan, Siberian plateau, etc.). Large volumes of magmatic rocks were first produced and then weathered. The short-lived ocean anoxic events at the Permo-Triassic or Cretaceous-Paleogene transitions are temporally related to LIP volcanism. Modelling of anoxic events could potentially be refined by testing for a short-period $\delta^{98/95}$Mo modification, which could be attributed to a weathering "peak". As another example, physical weathering during large glaciations could lead to non-steady-state intensive sulfide weathering on the newly exposed rock surfaces. This is in line with the observation of an increased Mo concentration in the Tista river (Neubert et al., 2011), which was interpreted by the authors as physical weathering by a glacier. In any case, it remains to be established if disseminated sulfide minerals generally have a heavier Mo isotopic composition than the coexisting silicates because of equilibrium fractionation, or if this effect is restricted to basalts. In

this respect, the study presented here is rather an identification of a process than the quantification of a Mo source.

6. Conclusions

The combined results of natural samples and bulk rock leaching experiments have identified bedrock-controlled heavy aquatic $\delta^{98/95}$Mo in a catchment underlain exclusively by igneous crustal rocks. The most important finding concerns the weathering of the basaltic bedrock, which dominates the dissolved Mo geochemistry in the catchment basin. While the basalts display a bulk rock signature with a $\delta^{98/95}$Mo ~ 0.1 ‰, the basalt leach solutions are enriched in the heavy isotopes. The consistency between these experimental data and the stream water $\delta^{98/95}$Mo are evidence that incongruent catchment outcrop weathering generates heavy isotope signatures of river dissolved Mo. Mass balance calculations based on LA-ICP-MS data of individual rock phases indicate that the preferential dissolution of magmatic sulfides drives the river dissolved load towards the observed heavy $\delta^{98/95}$Mo values. Consequently, the magmatic sulfides need to have prominently fractionated Mo isotopes relative to coexisting silicates. This makes it likely that Mo isotope fractionation also occurs at magmatic conditions similarly to reports of Fe fractionation in magmatic systems. Oxidative weathering of igneous crustal rocks can thus produce substantial Mo isotope fractionation through preferential dissolution of magmatic sulfides. It is clear, however, that the effect of incongruent chemical rock weathering strongly depends on primary rock composition, as illustrated by the significant differences in leach behavior of the three crustal bedrock types found in the study area. The excellent match between the $\delta^{98/95}$Mo values from the experiments and stream water samples deemphasizes soil formation, vegetation, adsorption processes and secondary mineral formation as important contributors to the

overall Mo isotope budget of the catchment studied here. On a global scale, the total weathered rock volume at any given time is limited. If light Mo isotopes are preferentially retained in weathering residues, erosion will liberate them sooner or later. Thus, whenever the globally integrated incongruent weathering of sulfide bearing fresh rocks is balanced by erosion of already weathered rocks, the Mo isotope effect will be zero. However, during periods of Earth's history when the Earth system was exceptionally far from steady state, incongruent weathering may have influenced the global continental runoff significantly. Conceivable examples are periods of large subaereal basalt eruptions (e.g., Deccan, Siberian plateau), or physical weathering related to large glaciations, with intensive sulfide weathering on the newly exposed rock surfaces. This study reiterates the importance of (igneous) bedrock weathering for the aquatic $\delta^{98/95}$Mo signature, while at the same time acknowledging the role of all other processes which contribute to a heavy aquatic Mo signature. River water $\delta^{98/95}$Mo signatures are thus expected to be variable in space and time and may be controlled by processes of incongruent magmatic rock weathering.

Acknowledgements

This work was financed by funds from the Swiss National Science Foundation (Grant 200021-126759 and 200020-113658). Special thanks go to Ulrich Linden for his tremendous help during field work. Ludovic Chaux and Thomas Routier kindly provided us with rock samples. We thank Priska Bähler for anion and cation determinations, as well as Barbara Zihlmann for XRD analysis. Nicolas Greber and Pierre Dèzes are acknowledged for their constructive comments on language and outline. This manuscript benefited from the comments of two anonymous reviewers.

List of Figures

1 Geological sketch map of the study area (modified after Steinmann & Stille, 2008) indicating water, rock and soil sampling locations along the Malaval and Séjallières streams. 29

2 Mo isotopic compositions of stream waters collected in June 2003 and June 2010. Grey shaded area = Mo isotopic variability of basalt leach solutions. 30

3 Mo isotopic compositions and concentrations of bulk rock samples. Analyses were done on separate sample splits. Variability of $\delta^{98/95}$Mo data is attributed to inhomogeneities of the sample material (external reproducibility of the analytical procedure = ±0.1 ‰ 2σ). Dark shaded area = range of crustal igneous rocks $\delta^{98/95}$Mo values after Siebert et al. (2003). 31

4 Results of leach experiments of basalt sample PA-1. Dark shaded area = range of bulk rock $\delta^{98/95}$Mo, medium shade area = percentage range of leach solutions dominated by sulfide dissolution, light shaded area = range of river water $\delta^{98/95}$Mo of the Séjallières and the Malaval. Dotted lines = transition between sulfide dominance and matrix dominance in leach solutions (see text for details), solid line = $\delta^{98/95}$Mo trend of basalt solutions to be expected at increasing leach rates and thus increasing rock matrix influence, dashed line = bulk rock $\delta^{98/95}$Mo (median). 32

5 Results of granite (A), basalt (B) and orthogneiss (C) leach experiments. All experiments were done using HNO_3 as leaching agent. Dashed line = bulk rock $\delta^{98/95}$Mo (median). Dark shaded area = range of bulk rock $\delta^{98/95}$Mo, light shaded area = range of stream water $\delta^{98/95}$Mo of the Séjallières and the Malaval. 33

6 Time dependence of Mo release during basalt leach experiments. (A) Powder leach; right axis = 2 mol L^{-1} HNO_3 leach of sample PA-1; left axis = 0.3 and 2 mol L^{-1} HNO_3 leach of M29-R and 0.3 mol L^{-1} HNO_3 leach of PA-1. (B) Grain leach; left axis = Mo concentrations, right axis= sulfate concentrations. Note the proportionality between both. The Mo concentrations of the 2 mol L^{-1} HNO_3 powder leaches (PA-1) are plotted on the right side axis due to their higher Mo concentrations. Grain and strong acid leach experiments produce increasing Mo concentrations. The weak acid experiments produce Mo concentrations which decrease with time. 34

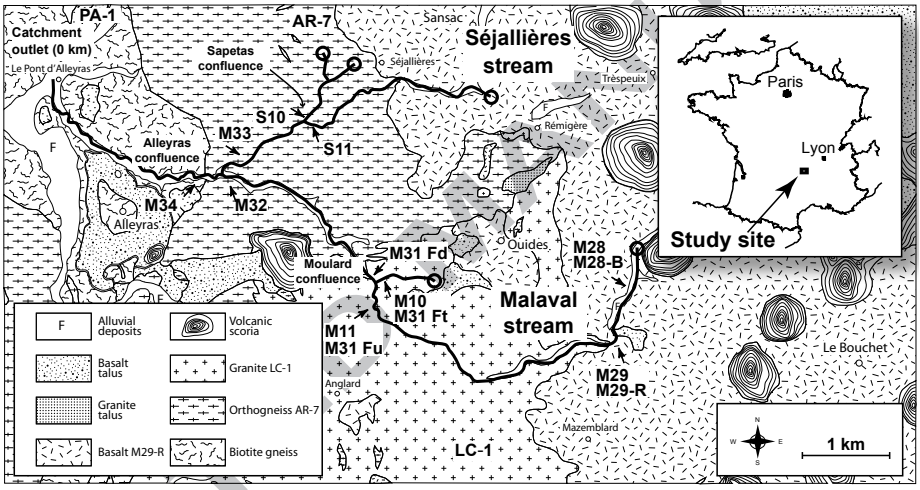

Figure 1:

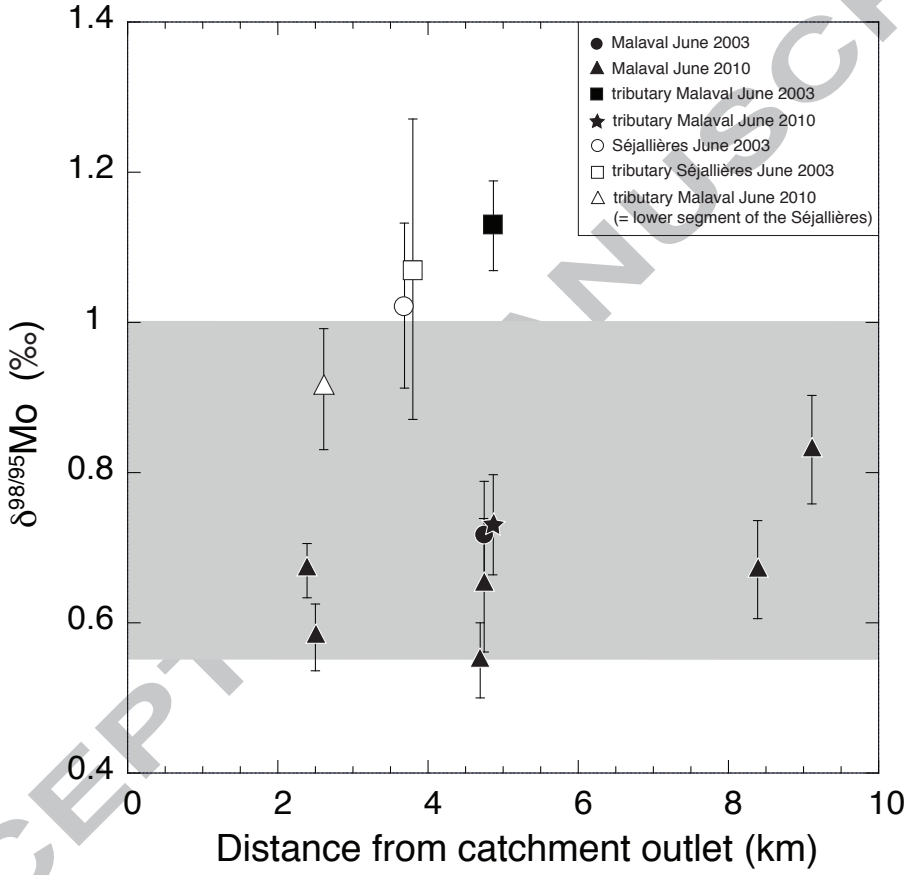

Figure 2:

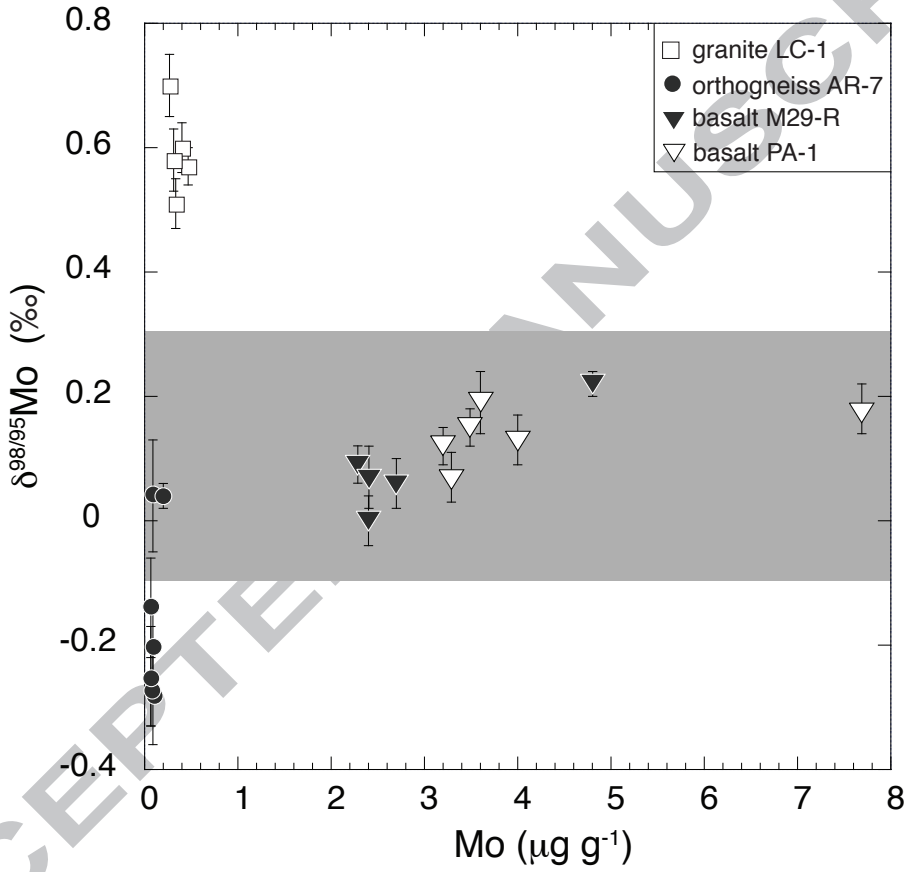

Figure 3:

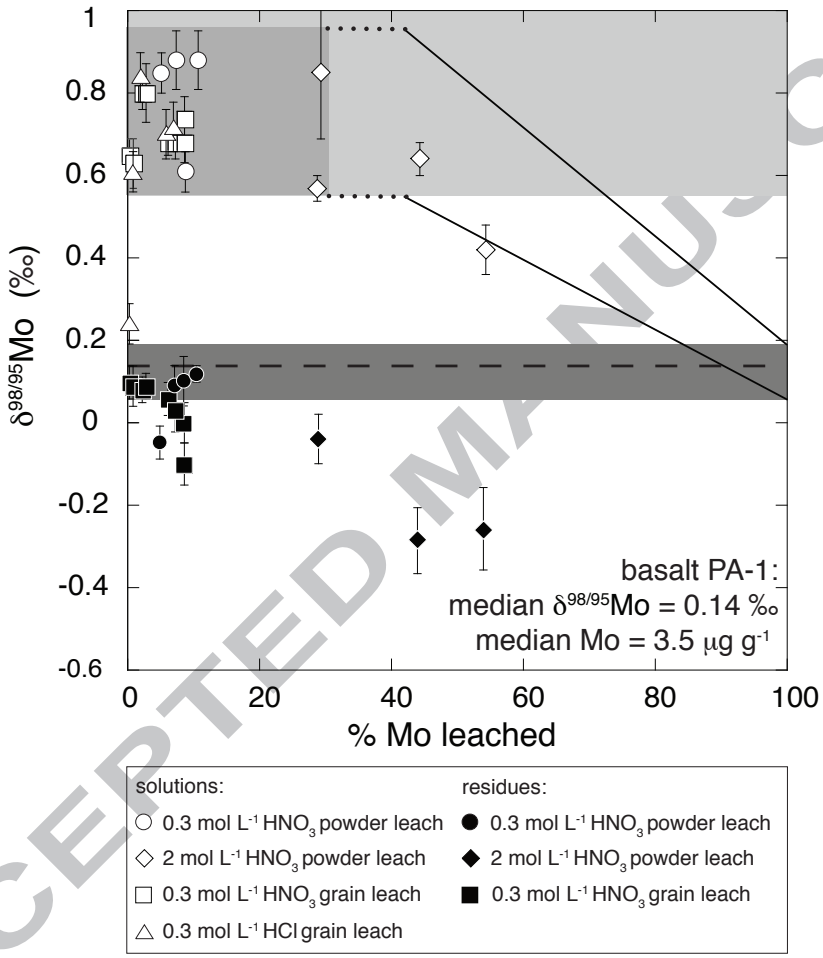

Figure 4:

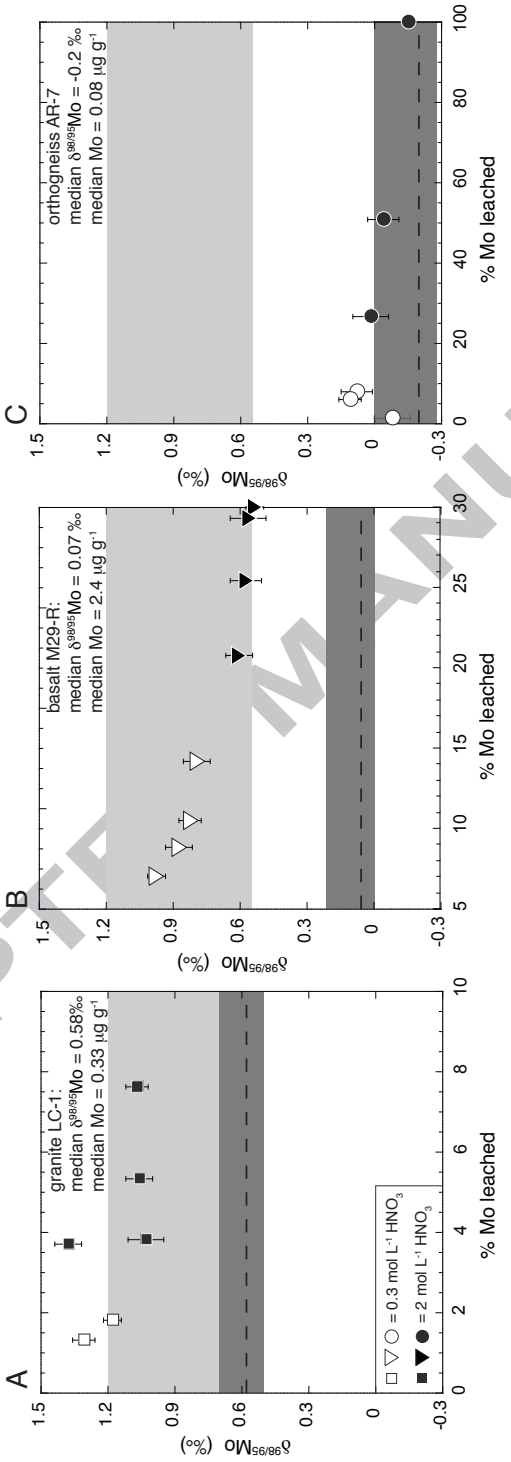

Figure 5:

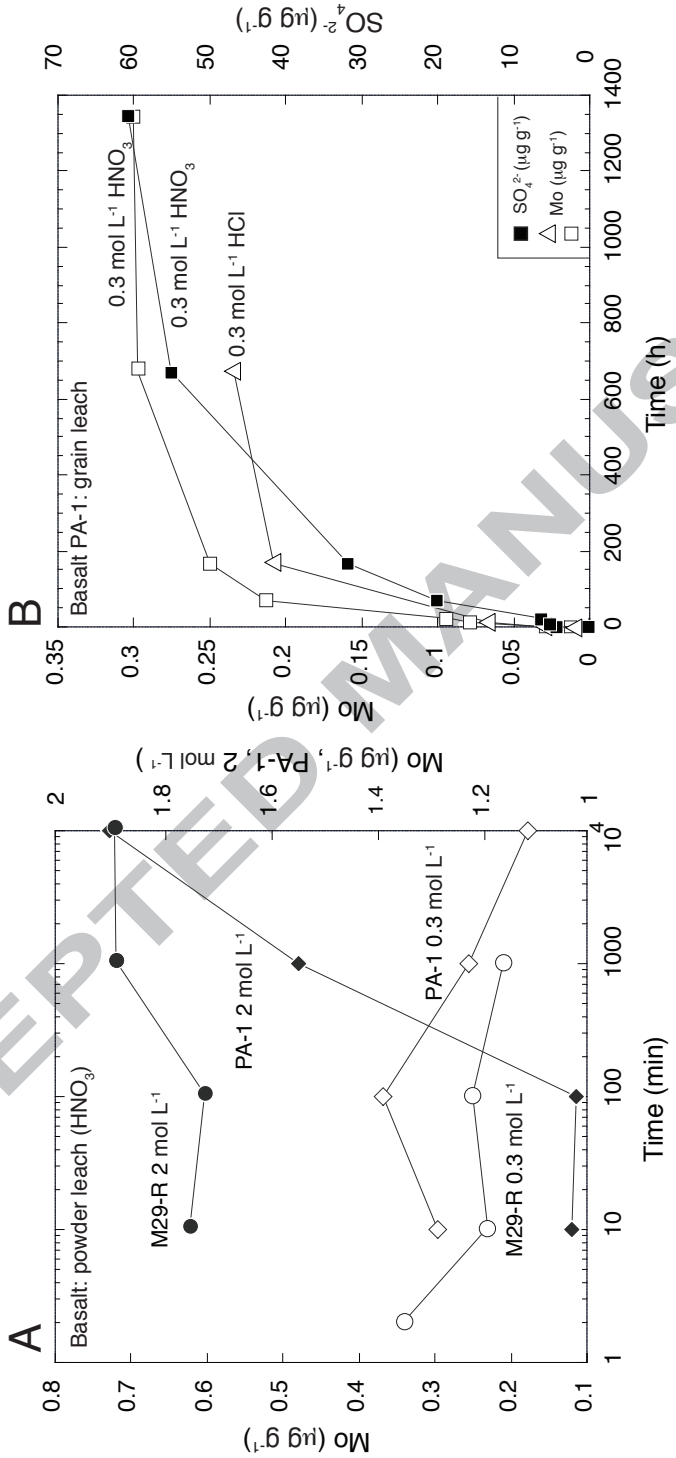

Figure 6:

List of Tables

1 Dissolved Mo and Sr isotopic compositions and dissolved Mo concentrations of stream water samples (<0.45 μm fraction). GSC = granite, OG = orthogneiss, BA = basalt. The 2σ external reproducibility of the Mo-isotope data is ±0.1 ‰. 37

2 Field parameters (pH, Eh, conductivity, temperature) and chemical composition for river water samples, filtered using 0.22 μm filters. June 2003 data are taken from Steinmann & Stille (2008) 38

3 Mo and Sr data of bulk rock samples. All analyses were done on separate sample splits. Variations in $\delta^{98/95}$Mo are attributed to moderate sample heterogeneity. The 2σ external reproducibility of the Mo-isotope data is ±0.1 ‰. Nugget effects cause the data distribution to be non-gaussian. Therefore, the median rather than the arithmetic mean is used for rock Mo concentrations and isotopic compositions as it gives a better indication of tendency. 39

4 Average Mo concentrations of single minerals and the basalt matrix of sample PA-1 determined by LA-ICP-MS. See section 4.2 for more details on data range. The missing Mo in the mass balance is attributed to the sulfide melt inclusions (Tables 5 and 9). 40

5 LA-ICP-MS data of sulfidic melt inclusions of basalt sample PA-1. 40

6 Mo data of root and soil material. 40

7 Weight of suspended particles extracted from stream waters using 0.45μ filters. 41

8 Results of leach experiments conducted on basaltic and granitic bedrock samples. The uncertainty on the Mo concentration in the leachate is 0.5%. However, the uncertainty on the mass balance of the leached mass fraction is estimated at 20% based on the observed inhomogeneity of the Mo concentration in the bulk rock. 42

9 Model parameters and mass balance calculations. Concentrations values for oxides, silicates and the matrix were kept constant based on results of LA-ICP-MS data. Modal abundances used were cross-checked with results of optically determined values (see Table 4). 43

Table 1:

	Rock type	Upstream distance [km]	$\delta^{98/95}$Mo [‰]	2SE[a]	Mo [ng g^{-1}]	^{87}Sr/^{86}Sr	2SE[a]
Water Samples June 2003							
M10	GSC	4.9	1.13	0.06	0.81	0.709749[b]	10
M11	GSC	4.8	0.72	0.07	0.30	0.706340[b]	10
S10	OG	3.8	1.07	0.20	0.20	0.704790[b]	10
S11	OG	3.7	1.02	0.11	0.17	0.704450[b]	10
Water Samples June 2010							
M28	BA	8.9	0.83	0.07	0.02	0.703853	36
M29	BA	8.4	0.67	0.07	0.04	0.703759	34
M31-Ft	GSC	4.9	0.73	0.07	0.15	0.709332	28
M31-Fu	GSC	4.8	0.65	0.09	0.12	0.705535	24
M31-Fd	GSC	4.7	0.55	0.01	0.12	0.705692	38
M32	OG	2.5	0.58	0.05	0.15	0.705322	34
M33	OG	2.6	0.91	0.08	0.07	0.704813	26
M34	OG	2.4	0.67	0.04	0.14	0.705175	38

[a] 2SE of individual measurements, the external reproducibility of the analytical procedure is ±0.1‰ (2σ). The 2SE of the Sr-isotope ratios refer to the last two digits.
[b] ^{87}Sr/^{86}Sr data from Steinmann & Stille (2008).

Table 2:

	Upstream distance [km]	Rock type	pH	Eh [mV]	EC [$\mu S\ cm^{-1}$]	T [°C]	F^- [$mg\ L^{-1}$]	Cl^- [$mg\ L^{-1}$]	NO_3^- [$mg\ L^{-1}$]	SO_4^{2-} [$mg\ L^{-1}$]	HCO_3^- [$mg\ L^{-1}$]	Ca^{2+} [$mg\ L^{-1}$]	Na^+ [$mg\ L^{-1}$]	K^+ [$mg\ L^{-1}$]	Mg^{2+} [$mg\ L^{-1}$]	Charge Balance
Water samples June 2003																
M10	4.9	GSC	7.7	180	168	14.5	0.20	2.8	0.7	6.8	95	14.9	11.3	1.0	6.5	0.0 %
M11	4.8	GSC	7.5	265	95	12.8	0.09	3.3	2.5	5.9	36	5.6	5.3	0.9	4.6	-4.1 %
S10	3.8	OG	8.2	250	188	16.8	0.05	7.5	3.1	5.5	89	13.4	7.6	4.9	11.6	-6.7%
S11	3.7	OG	8.1	258	174	14.5	0.07	6.9	8.1	5.9	73	11.0	5.4	3.3	11.1	-4.0%
Water samples June 2010																
M28	9.1	BA	7.0	220	40	9.4	0.00	1.3	0.5	1.7	41	4.6	4.2	0.1	4.0	0.7%
M29	8.4	BA	8.1	160	77	9.3	0.00	2.3	2.3	2.4	51	6.0	3.4	0.3	5.0	6.5%
M31-Ft	4.9	GSC	-	-	-	-	<0.50	4.8	-	7.3	-	6.3	4.2	<1	3.2	-
M31-Fu	4.8	GSC	-	-	-	-	<0.50	3.2	3.8	5.7	-	6.3	4.1	<1	4.7	-
M31-Fd	4.7	GSC	7.9	280	82	10.3	0.15	3.0	4.5	5.2	44	5.8	6.8	0.6	4.6	0.4%
M32	2.5	OG	8.1	-	98	11.6	0.18	3.2	4.8	5.7	51	7.8	6.4	0.9	5.6	-0.9%
M33	2.6	OG	8.3	-	121	12.1	0.16	3.4	4.3	6.8	67	8.6	4.8	1.1	7.8	3.5%
M34	2.4	OG	8.2	-	105	11.9	0.16	3.3	4.7	5.9	54	7.6	5.2	0.9	6.2	1.4%

Table 3:

Split	$\delta^{98/95}$Mo [‰]	2SE[a]	Mo [μg g^{-1}]	^{87}Sr/^{86}Sr
Basalt: PA-1				
1	0.15	0.03	3.5	-
2	0.07	0.04	3.3	-
3	0.18	0.04	7.7	-
4	0.19	0.05	3.6	-
5	0.12	0.03	3.2	-
6	0.13	0.04	4.0	-
Median	0.14		3.5	-
Basalt: M29-R				
1	0.07	0.05	2.4	-
2	0.09	0.03	2.3	-
3	0.06	0.04	2.7	-
4	0.22	0.02	4.8	
5	0.00	0.04	2.4	
Median	0.07		2.4	0.703348±12[b]
Orthogneiss: AR-7				
1	-0.25	0.08	0.07	-
2	0.04	0.02	0.19	-
3	-0.28	0.08	0.08	-
4	0.04	0.09	0.09	-
5	-0.20	0.06	0.08	-
6	-0.27	0.06	0.07	-
7	-0.14	0.08	0.07	-
Median	-0.2		0.08	0.751991±13[b]
Granite: LC-1				
1	0.57	0.03	0.47	-
2	0.70	0.05	0.26	-
3	0.60	0.04	0.41	-
4	0.58	0.05	0.31	-
5	0.51	0.04	0.33	-
Median	0.58		0.33	0.722319±13[b]

[a] 2SE of individual measurements, the external reproducibility of the analytical procedure is ±0.1‰ (2σ)

[b] typical ^{87}Sr/^{86}Sr values taken from Steinmann & Stille (2008). 2SE of the Sr-isotope ratios refer to the last two digits.

Table 4:

Mineral Phase	avg. Mo [μg g^{-1}]	1SE	Modal abundances[a]	Model parameters
Olivine	0.14	0.03		
Pyroxene (cpx)	0.14	0.03	15% – 20%	15%
Plagioclase	1.25	0.43		
Titanomagnetite	0.92	0.18	3% – 7%	5%
Matrix	3.53	0.69	75% – 80%	79.2 – 79.5%

[a]determined by optical microscopy

Table 5:

Analysis No.	Mo [μg g^{-1}]	S [a] [wt%]	Fe [wt%]	Cu [wt%]	Ni [wt%]	Zn [μg g^{-1}]	Ti [μg g^{-1}]	Pb [μg g^{-1}]	Fe/Cu	Ni/Cu
Inclusion type 1										
26ala03.xl	1.1	29	60	0.5	3.2	140	440	<0.2	123	6.6
26ala04.xl	1.5	29	61	0.3	2.8	150	71	<0.2	239	10.9
26ala05.xl	1.1	27	60	0.4	3.6	170	210	<0.4	165	10.0
26ala06.xl	<0.05	28	60	0..5	3.0	180	660	<0.6	117	5.9
Inclusion type 2										
26ala07.xl	2.0	22	53	7.6	3.4	320	2700	140	7	0.4
26ala08.xl	0.8	28	59	1.5	3.5	60	<93	<1	39	2.3
26ala09.xl	200	22	57	4.3	2.4	360	22000	15	13	0.6
26ala10.xl	22.0	29	61	1.7	1.0	103	<50	2	36	0.6
26ala11.xl	52.4	30	61	1.6	1.1	99	<40	6	38	0.7
26ala12.xl	39.8	33	61	1.6	1.1	103	2900	<3	37	0.7
26alc14.xl	0.3	18	60	1.2	2.6	260	1700	0.2	50	2.2
26alc15.xl	2.0	21	60	2.0	2.0	300	250	4	30	1.0
24mrb06.xl	250	27	61	1.5	0.8	150	<1000	1	42	0.5
Inclusion type 3										
24mrb03.xl	35	25	34	30	0.7	430	<84	320	1.2	0.0
24mrb05.xl	78	23	29	35	1.1	750	<44	670	0.8	0.0
24mrb07.xl	28	23	30	32	3.1	740	44000	500	0.9	0.1
24mrb09.xl	16	22	32	28	4.4	1500	<263	30	1.1	0.2

[a]calculated based on (Fe, Ni, Cu)S stoichiometry

Table 6:

Sample	Type	$\delta^{98/95}$Mo	2SE [‰]	Mo [μg g^{-1}]
M28-B	top soil	-0.33	0.1	2.38
M28-BW	root material	-0.14	0.0	0.67

Table 7:

	Upstream distance [km]	Rock type	Suspension weight [mg L^{-1}]
Samples June 2003			
M10	4.9	GSC	1.3 [a]
M11	4.8	GSC	5.5[a]
S10	3.8	OG	19.7 [a]
S11	3.7	OG	5.6[a]
Samples June 2010			
M28	8.9	BA	b.d.l.
M29	8.4	BA	b.d.l.
M31-Ft	4.9	GSC	b.d.l.
M31-Fu	4.8	GSC	b.d.l.
M31-Fd	4.7	GSC	b.d.l.
M32	2.5	OG	b.d.l.
M33	2.6	OG	b.d.l.
M34	2.4	OG	b.d.l.

[a]2003 data taken from Steinmann & Stille (2008)

Table 8:

leach time	leaching agent	Temp.	Mo leached [%]	$\delta^{98/95}$Mo in solution [‰]	2SE	Mo in solution [μg g^{-1}]^a	$\delta^{98/95}$Mo in residue [‰]	2SE	SO_4^{2-} in solution [μg g^{-1}]^a	$\delta^{98/95}Mo_{MB}$ [‰]^b
Basalt: PA-1 grain leach										
10min	0.3 mol L^{-1} HNO_3	cold	0.4	0.65	0.04	0.01	0.10	0.04	b.d.l.	-0.04
0.5h	0.3 mol L^{-1} HNO_3	cold	0.8	0.63	0.06	0.03	0.09	0.05	4.4	-0.05
12h	0.3 mol L^{-1} HNO_3	cold	2.3	0.80	0.04	0.08	0.08	0.03	5.6	-0.05
24h	0.3 mol L^{-1} HNO_3	cold	2.7	0.80	0.07	0.09	0.09	0.03	6.3	-0.04
72h	0.3 mol L^{-1} HNO_3	cold	6.1	0.68	0.03	0.21	0.06	0.04	20.0	-0.05
1w	0.3 mol L^{-1} HNO_3	cold	7.1	0.68	0.04	0.25	0.03	0.05	31.7	-0.07
1m	0.3 mol L^{-1} HNO_3	cold	8.5	0.68	0.05	0.30	-0.10	0.05	55.0	-0.18
2m	0.3 mol L^{-1} HNO_3	cold	8.7	0.74	0.05	0.30	0.00	0.05	61.7	-0.09
10min	0.3 mol L^{-1} HCl	cold	0.3	0.24	0.05	0.01	-	-	-	-
0.5h	0.3 mol L^{-1} HCl	cold	0.8	0.61	0.05	0.03	-	-	-	-
12h	0.3 mol L^{-1} HCl	cold	1.9	0.84	0.06	0.07	-	-	-	-
1w	0.3 mol L^{-1} HCl	cold	5.8	0.70	0.06	0.21	-	-	-	-
1m	0.3 mol L^{-1} HCl	cold	7.0	0.72	0.06	0.23	-	-	-	-
Basalt: PA-1 powder leach										
10min	0.3 mol L^{-1} HNO_3	cold	8.5	0.61	0.05	0.30	0.10	0.06	-	0.00
100min	0.3 mol L^{-1} HNO_3	cold	10.5	0.88	0.07	0.37	0.12	0.02	-	0.05
1000min	0.3 mol L^{-1} HNO_3	cold	7.3	0.88	0.07	0.26	0.09	0.05	-	0.00
10'000min	0.3 mol L^{-1} HNO_3	cold	5.1	0.85	0.05	0.18	-0.05	0.04	-	-0.15
10min	2 mol L^{-1} HNO_3	50°C	28.6	0.57	0.03	1.03	-	-	-	-
100min	2 mol L^{-1} HNO_3	50°C	29.2	0.85	0.16	1.02	-0.04	0.06	-	0.03
1000min	2 mol L^{-1} HNO_3	50°C	44.1	0.64	0.04	1.54	-0.29	0.08	-	-0.09
10'000min	2 mol L^{-1} HNO_3	50°C	54.3	0.42	0.06	1.90	-0.26	0.10	-	-0.09
Basalt: M29-R powder leach										
2min	0.3 mol L^{-1} HNO_3	cold	14.2	0.79	0.06	0.34	-	-	-	-
10min	0.3 mol L^{-1} HNO_3	cold	7.0	0.97	0.04	0.23	-	-	-	-
100min	0.3 mol L^{-1} HNO_3	cold	10.5	0.82	0.05	0.25	-	-	-	-
1000min	0.3 mol L^{-1} HNO_3	cold	8.8	0.87	0.06	0.21	-	-	-	-
10min	2 mol L^{-1} HNO_3	50°C	25.4	0.57	0.07	0.62	-	-	-	-
100min	2 mol L^{-1} HNO_3	50°C	20.8	0.60	0.06	0.60	-	-	-	-
1000min	2 mol L^{-1} HNO_3	50°C	29.4	0.56	0.08	0.72	-	-	-	-
10'000min	2 mol L^{-1} HNO_3	50°C	30.0	0.53	0.04	0.72	-	-	-	-
Orthogneiss: AR-7 powder leach										
10min	0.3 mol L^{-1} HNO_3	cold	7.9	0.08	0.07	0.01	-	-	-	-
100min	0.3 mol L^{-1} HNO_3	cold	6.3	0.11	0.05	0.005	-	-	-	-
10'000min	0.3 mol L^{-1} HNO_3	cold	1.4	-0.08	0.10	0.001	-	-	-	-
100min	2 mol L^{-1} HNO_3	50°C	26.8	0.02	0.08	0.02	-	-	-	-
1000min	2 mol L^{-1} HNO_3	50°C	50.9	-0.04	0.07	0.04	-	-	-	-
10'000min	2 mol L^{-1} HNO_3	50°C	100	-0.15	0.15	0.10	-	-	-	-
Granite: LC-1 powder leach										
10min	0.3 mol L^{-1} HNO_3	cold	1.8	1.18	0.04	0.01	-	-	-	-
100min	0.3 mol L^{-1} HNO_3	cold	1.3	1.31	0.05	0.004	-	-	-	-
10min	2 mol L^{-1} HNO_3	50°C	3.7	1.38	0.06	0.01	-	-	-	-
100min	2 mol L^{-1} HNO_3	50°C	3.8	1.03	0.08	0.01	-	-	-	-
1000min	2 mol L^{-1} HNO_3	50°C	5.3	1.06	0.06	0.02	-	-	-	-
10'000min	2 mol L^{-1} HNO_3	50°C	7.6	1.07	0.05	0.03	-	-	-	-

[a] Concentrations relative to grams of sample material leached.

[b] difference between bulk rock $\delta^{98/95}$Mo composition and $\delta^{98/95}$Mo composition of calculated mass balance.

Table 9:

Modal abundances				**Concentrations**					**Fraction of bulk rock Mo inventory**			
oxides [%]	sulfides[a] [%]	phenocrysts[b] [%]	matrix [%]	oxides [μg g^{-1}]	sulfides [μg g^{-1}]	phenocrysts[b] [μg g^{-1}]	matrix [μg g^{-1}]	Total [μg g^{-1}]	oxides [%]	sulfides [%]	phenocrysts[b] [%]	matrix [%]
5	0.5	15	79.5	1.0	40	0.5	3.5	3.1	1.6	6.5	2.4	89.5
5	0.5	15	79.5	1.0	70	0.5	3.5	3.2	1.5	10.8	2.3	85.3
5	0.5	15	79.5	1.0	100	0.5	3.5	3.4	1.5	14.8	2.2	81.6
5	0.5	15	79.5	1.0	150	0.5	3.5	3.6	1.4	20.6	2.1	76.0
5	0.8	15	79.2	1.0	40	0.5	3.5	3.2	1.6	10.0	2.3	86.1
5	0.8	15	79.2	1.0	70	0.5	3.5	3.5	1.5	16.2	2.2	80.1
5	0.8	15	79.2	1.0	100	0.5	3.5	3.7	1.4	21.7	2.0	75.0
5	0.8	15	79.2	1.0	150	0.5	3.5	4.1	1.2	29.3	1.8	67.7

[a]total content <1% based on XRD analysis
[b]sum of plagioclase, pyroxene and olivine

ACCEPTED MANUSCRIPT

764 Anbar, A. D., Knab, K. A. and Barling, J. (2001) Precise determination of
765 mass-dependent variations in the isotopic composition of molybdenum using
766 MC-ICPMS. *Anal. Chem.* **73**, 1425–1431.

767 Anbar, A. D., Duan, Y., Lyons, T. W., Arnold, G. L., Kendall, B., Creaser,
768 R. A., Kaufman, A. J., Gordon, G. W., Scott, C., Garvin, J. and Buick, R.
769 (2007) A whiff of oxygen before the great oxidation event? *Science* **317**,
770 1903–1906.

771 Archer, C. and Vance, D. (2008) The isotopic signature of the global riverine
772 molybdenum flux and anoxia in the ancient oceans. *Nature Geosci.* **1**, 597–
773 600.

774 Arnold, G. L., Anbar, A. D., Barling, J. and Lyons, T. W. (2004) Molybdenum
775 isotope evidence for widespread anoxia in mid-Proterozoic oceans. *Science*
776 **304**, 87–90.

777 Arnórsson, S. and Oskarsson, N. (2007) Molybdenum and tungsten in volcanic
778 rocks and in surface and <100°C ground waters in Iceland. *Geochim. Cos-*
779 *mochim. Acta* **71**, 284–304.

780 Audétat, A. (2010) Source and evolution of molybdenum in the porphyry Mo(-
781 Nb) deposit at Cave Peak, Texas. *J. Petrol.* **51**, 1739–1760.

782 Barling, J., Arnold, G. L. and Anbar, A. D. (2001) Natural mass-dependant
783 variations in the isotopic composition of molybdenum. *Earth Planet. Sci.*
784 *Lett.* **193**, 447–457.

785 Barling, J. and Anbar, A. D. (2004) Molybdenum isotope fractionation during
786 adsorption by manganese oxides. *Earth Planet. Sci. Lett.* **217**, 315–329.

787 Binet, S., Spadini, L., Bertrand, C., Guglielmi, Y., Mudry, J. and Scavia, C.
788 (2009) Variability of the groundwater sulfate concentration in fractured rock

slopes: a tool to identify active unstable areas.. *Hydrol. Earth Syst. Sci.* **13**, 2315–2327.

Cenki-Tok, B., Chabaux, F., Lemarchand, D., Schmitt, A.-D., Pierret, M.-C., Viville, D., Bagard, M.-L. and Stille, P. (2009) The impact of water-rock interaction and vegetation on calcium isotope fractionation in soil- and stream waters of a small, forested catchment (the Strengbach case). *Geochim. Cosmochim. Acta* **73**, 2215–2228.

Cruywagen, J. J. and Heyns, J. B. B. (1989) Spectrophotometric determination of the thermodynamic parameters for the first two protonation reactions of molybdate. *J.Chem. Educ.* **66**, 861–863.

Cruywagen, J. J. and Heyns, J. B. B. (2000) Molybdenum (VI) equilibria at high perchloric acid concentration. *Polyhedron* **19**, 907–911.

Eggins, S. M. and Shelley, J. M. G. (2002) Compositional heterogeneity in NIST SRM 610-617 glasses. *Geostandards Newslett.* **26**, 269–286.

Fitzpatrick, K. L., Tyerman, S. D. and Kaiser, B. N. (2008). Molybdate transport throught the plant sulfate stranporter SHST1. *FEBS Lett.* **582**, 1508–1513.

Gaillardet, J., Viers, J. and Dupré, B. (2003) Trace elements in river waters In *Treatise in Geochemistry* (eds. E. D. Holland and K. K. Turekian). **5**, 225–272. Elsevier-Pergamon.

Garrels, R. M. and Mackenzie, F. T. (1971) *Evolution of Sedimentary Rocks*. Norton.

Gislason, S. R. and Eugster, H. P. (1987) Meteoric water-basalt interactions: I. a laboratory study. *Geochim. Cosmochim. Acta* **51**, 2827–2840.

Goldberg, S., Forster, H. S. and Godfrey, C. L. (1996) Molybdenum adsorption on oxides, clay minerals, and soils. *Soil Sci. Soc. Am. J.* **60**, 425–432.

Goldberg, T., Archer, C., Vance, D. and Poulton, S. W. (2009) Mo isotope fractionation during adsorption to Fe (oxyhydr)oxides. *Geochim. Cosmochim. Acta* **73**, 6502–6516.

Guillong, M., Meier, D. L., Allan, M. M., Heinrich, C. A. and Yardley, B. W. D. (2008) Sills: A matlab-based program for the reduction of laser ablation ICP-MS data of homogenous materials and inclusions. In *Laser Ablation ICP-MS in the Earth Sciences: Current Practices and Outstanding Issues* (ed. P. Sylvester). Mineralogical Association of Canada Volume 40 of Short Course Series, pp. 328–333.

Halter, W. E., Pettke, T., Heinrich, C. A. and Rothen-Rutishauser, B. (2002) Major to trace element analysis of melt inclusions by laser-ablation ICP-MS: methods of quantification. *Chem. Geol.* **183**, 63–86.

Johnson, C. M., Beard, B. L., Roden, E. E., Newman, D. K. and Nealson, K. H. (2004) Isotopic constraints on biogeochemical cycling of Fe. *Rev. Mineral. Geochem.* **55**, 359–408.

Kawakubo, S., Hashi, S. and Iwatsuki, M. (2001) Physicochemical speciation of molybdenum in rain water. *Water Res.* **35**, 2489–2495.

Kim, M.-J. and Jang, M. (2010) Adsorption of molybdate onto hematite: Kinetics and equilibrium. In *Water and Geoscience* (eds. E. D. Schmitter and N. Mastorakis). Cambridge: WSEAS Press, pp. 170–173.

Liermann, L. J., Mathur, R., Wasylenki, L. E., Nuester, J., Anbar, A. D. and Brantley, S. L. (2011) Extent and isotopic composition of Fe and Mo release

from two Pennsylvanian shales in the presence of organic ligand and bacteria. *Chem. Geol.* **281**, 167–180.

McManus, J., Berelson, W. M., Severmann, S., Poulson, R. L., Hammond, E., Douglas, Klinkhammer, G. P. and Holm, C. (2006) Molybdenum and uranium geochemistry in continental margin sediments: Paleoproxy potential. *Geochim. Cosmochim. Acta* **70**, 4643–4662.

McManus, J., Nägler, T. F., Siebert, C., Wheat, C. G. and Hammond, D. E. (2002) Oceanic molybdenum isotope fractionation: Diagenesis and hydrothermal ridge-flank alteration. *Geochem. Geophy. Geosy.* **3**.

Mendel, R. R. and Bittner, F. (2006) Cell biology of molybdenum. *Biochim. Biophys. Acta* **1763**, 621–635.

Morford, J. L. and Emerson, S. (1999) The geochemistry of redox sensitive trace metals in sediments. *Geochim. Cosmochim. Acta* **63**, 1735–1750.

Nägler, T. F., Siebert, C., Lüschen, H. and Böttcher, M. E. (2005) Sedimentary Mo isotope record across the Holocene fresh-brackish water transition of the Black Sea. *Chem. Geol.* **219**, 283–295.

Neubert, N., Heri, A. R., Voegelin, A. R., Nägler, T. F., Schlunegger, F. and Villa, I. M. (2011) The molybdenum isotopic composition in river water: Constraints from small catchments. *Earth Planet. Sci. Lett.* **304**, 180–190 .

Neubert, N., Nägler, T. F. and Böttcher, M. (2008) Sulfidity controls molybenum isotope fractionation into euxinic sediments: Evidence from the modern Black Sea. *Geology*, **36**, 775–778.

Ozeki, T., Adachi, H. and Ikeda, S. (1996) Estimation of the dissolved structures and condensation reactivities of mononuclear molybdenum (VI) species in

861 solution using the UV-vis absorption spectra and molecular orbital calculation
862 DV-$X\alpha$. *B. Chem. Soc. Jpn.* **69**, 619–625.

863 Pearce, C. R., Burton, K. W., Pogge von Strandmann, A. E., James, R. H.
864 and Gislason, S. R. (2010) Molybdenum isotope behaviour accompanying
865 weathering and riverine transport in a basaltic terrain. *Earth Planet. Sci.*
866 *Lett.* **295**, 104–114.

867 Pearce, C. R., Cohen, A. S., Coe, A. L. and Burton, K. W. (2008) Molybdenum
868 isotopie evidence for global ocean anoxia coupled with perturbations to the
869 carbon cycle during the early Jurassic. *Geology* **26**, 231–234.

870 Pettke, T. (2008) Analytical protocols for elment concentration and isotope
871 ratio measurement in fluid inclusions by LA-(MC)-ICP-MS. In *Laser Ablation*
872 *ICP-MS in the Earth Sciences: Current Practices and Outstanding Issues*
873 (ed. P. Sylvester). Mineralogical Association of Canada Volume 40 of Short
874 Course Series, pp. 189–218.

875 Pistiner, J. S. and Henderson, G. M. (2003) Lithium-isotope fractionation during
876 continental weathering processes. *Earth Planet. Sci. Lett.* **214**, 327–339.

877 Rudnick, R. L. and Gao, S. (2004) Composition of the Continental Crust *Trea-*
878 *tise in Geochemistry* (eds. E. D. Holland and K. K. Turekian). **3**, 1–64. Am-
879 sterdam: Elsevier.

880 Schuessler, J. A., Schoenberg, R., Behrens, H., & von Blanckenburg, F. (2007).
881 The experimental calibration of the iron isotope fractionation factore between
882 pyrrhotite and peralkaline rhyolitic melt. *Geochim. et Cosmochim. Acta*, **71**,
883 417–433.

884 Shahar, A., Young, E. D., and Manning, C. E. (2008) Equilibrium high-

temperature Fe isotope fractionation between fayalite and magnetite: An experimental calibration. *Earth Planet. Sci. Lett.* **268**, 330–338.

Siebert, C., Nägler, T. F. and Kramers, J. D. (2001) Determination of molybdenum isotope fractionation by double-spike multicollector inductively coupled plasma mass spectrometry. *Geochem. Geophy. Geosy.* **2**.

Siebert, C., Nägler, T. F., von Blanckenburg, F. and Kramers, J. D. (2003) Molybdenum isotope record as a potenial new proxy for paleoceanography. *Earth Planet. Sci. Lett.*, **211**, 159–171.

Siebert, C., Kramers, J. D., Nägler, T. F., Morel, P. and Berelson, W. M. (2005) PGE, Re-Os, and Mo isotope systematics in Archean and early Proterozoic sedimentary systems as proxies for redox conditions of the early Earth. *Geochim. et Cosmochim. Acta* **241**, 723–733.

Siebert, C., McManus, J., Bice, A., Poulson, R. and Berelson, W. M. (2006) Molybdenum isotope signatures in continental margin marine sediments. *Earth Planet. Sci. Lett.* **241**, 723–733.

Steinmann, M. and Stille, P. (2008) Controls on transport and fractionation of the rare earth elements in stream water of a mixed basaltic-granitic catchment basin (Massif Central, France). *Chem. Geol.* **254**, 1–18.

Tossel, J. A. (2005) Calculating the partitioning of the isotopes of Mo between oxidic and sulfidic species in aqueous solution. *Geochim. Cosmochim. Acta* **69**, 2981–2993.

Voegelin, A. R., Nägler, T. F., Beukes, N. J. and Lacassie, J. P. (2010) Molybdenum isotopes in late Archean carbonate rocks: Implications for early Earth oxygenation. *Precambrian Res.* **182**, 70–82.

Wille, M., Kramers, J. D., Nägler, T. F., Beukes, N. J., Schröder, S., Meisel, Th., Lacassie, J. P. and Voegelin, A. R. (2007) Evidence for a gradual rise of oxygen between 2.6 and 2.5 Ga from Mo isotopes and Re-PGE signatures in shales. *Geochim. Cosmochim. Acta* **71**, 2417–2435.

Xu, N., Christodoulatos, C. and Braida, W. (2006) Adsorption of molybdate and tetrathiomolybdate onto pyrite and goethite: Effect of ph and competitive anions. *Chemosphere* **62**, 1726–1735.

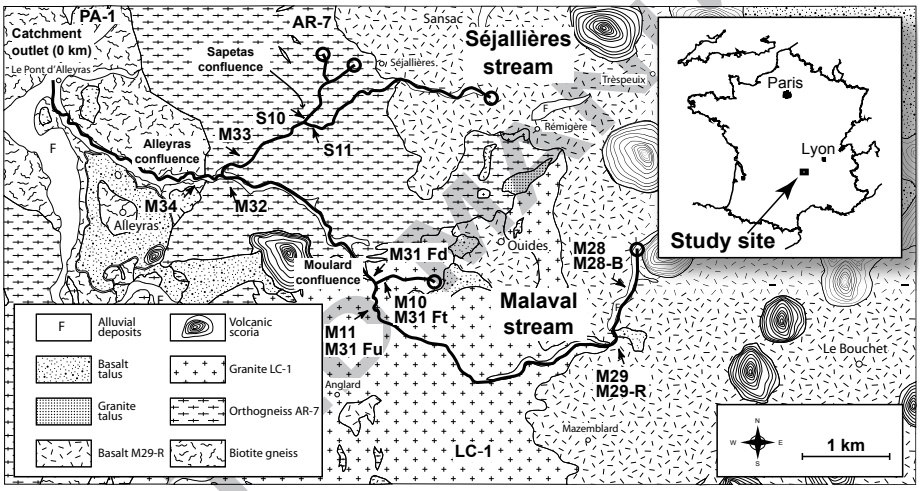

Figure 1: